JOURNAL OF MATERIALS SCIENCE 37 (2002) 2747–2753

# High-temperature reaction networks in graphite furnaces

KAI FENG, S. J. LOMBARDO
*Department of Chemical Engineering, University of Missouri-Columbia, Columbia, MO 65211, USA*
*E-mail: Lombardos@missouri.edu*

The intensity of gas-phase species present in a graphite furnace/dilatometer from room temperature to 1400°C were recorded by a mass spectrometer in real time. Based on the relative intensities and fragmentation factors, the species could be assigned to carbon dioxide, carbon monoxide, oxygen, water, and cyanogen. At low temperature, carbon dioxide was the main species observed whereas at high temperature, carbon monoxide was the predominant compound. The appearance of these species at low and high temperature was consistent with the results of equilibrium calculations for the coupled reactions of $C + O_2 = CO_2$ and $CO_2 + C = 2CO$. The intensity data from the mass spectrometer indicate that trace oxygen reacts with the graphite to form the carbon dioxide and carbon monoxide. 

## 1. Introduction

The identification of the gas-phase species that are evolved when inorganic materials are heated to high temperature has been carried out over the last 30 years by a number of techniques, and these have been reviewed in more detail elsewhere [1–4]. In one approach, a Knudsen diffusion cell containing a ceramic material is heated, and the reaction products which are evolved into the gas phase are either monitored directly by a mass spectrometer or trapped for subsequent analysis. A second technique has used a carrier gas flowing across a sample to transport the evolved species to the analytical device.

Although both of these techniques have supplied a wealth of information into the reactions that occur at high temperature, very little information has appeared in the literature as to the relationship between the reactions that occur at high temperature and the rate of sintering of ceramic powders. Questions that are of interest are to what extent, at what concentrations, and at what temperature species in the gas phase inhibit or enhance sintering kinetics. In addition to the reactions which may arise from the sample, the furnace environments in which samples are sintered contain materials which may participate in or catalyze reactions, and thus the extent to which these reactions occur is also of interest.

During the sintering of both oxide and non-oxide ceramics, different types of reactions involving gas-phase species may occur at high temperature. These reactions include the decomposition or dissociation of the inorganic material [4–6], the volatilization of sintering aids [7, 8], and the removal of native oxide surface films [9–11]. For non-oxide ceramics containing silicon, such as silicon nitride and silicon carbide, the occurrence of such reactions is more pronounced because of the high temperatures required for sintering. Silicon nitride, for instance, may dissociate when the temperature is too high or when the partial pressure of nitrogen is too low [12, 13]. Both the sintering and oxidation reactions of silicon-based materials also involve the surface oxide $SiO_2$ and gaseous SiO, and the relative amount of the two species depends on the partial pressure of oxygen. In addition, the formation of surface layers with different properties from the bulk for silicon nitride ceramics has also been widely reported [14]. Finally, the crucibles and powder beds used for sintering silicon nitride may also participate in high-temperature reaction networks and influence the microstructure of the material [13].

For silicon carbide materials, the participation of oxides of silicon and carbon in sintering and oxidation has also been reported. Ness and Rafaniello [11] have examined the origin of density gradients in $\beta$-silicon carbide bodies during sintering by periodically analyzing by gas chromatography a sample of gas removed from the hot zone. With this approach, they were able to correlate the evolution of CO with the occurrence of low density in the body.

Although high-temperature dilatometers [15–20] have been used to characterize the sintering of ceramic materials and mass spectrometers [5, 6, 21] have been used to characterize high-temperature reactions, these two techniques have not been routinely combined to simultaneously monitor the gas phase as sintering occurs. In this study, we have coupled a mass spectrometer to a dilatometer to detect gas-phase species that appear at high temperature. In the course of these investigations, we have observed that the reactions occurring at high temperature in the absence of any sample within the furnace are sufficiently complex that a thorough

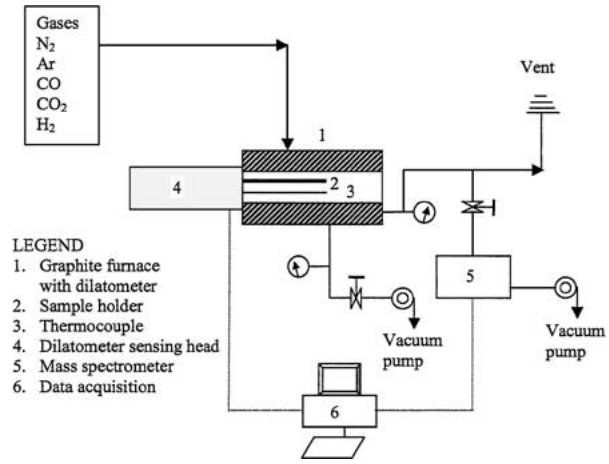


*Figure 1* Schematic of the experimental apparatus indicating the gas handling system, the furnace/dilatometer assembly, and the mass spectrometer.

understanding of the prevailing background reaction network is required before the more complex kinetics accompanying sintering can evaluated. This work reports on the experimental and modeling results obtained for the background reactions occurring at high temperature in graphite furnaces.

## 2. Experimental

The experimental apparatus is shown in Fig. 1 and consists of three sections: the gas handling system, the furnace/dilatometer assembly, and the mass spectrometer. The gas supply section consists of cylinders and a mixing station for preparing the desired gas-phase composition. The furnace/dilatometer (L75/2000, Linseis, Germany) can be heated to 2000°C and the temperature is measured by a type C thermocouple placed directly below the sample holder. The resistance furnace is constructed of graphite heating elements and graphite insulation and has a water-cooling jacket around the outer shell. The gas analysis section has a mass spectrometer (Hewlett Packard 5971, Palo Alto, CA) with an electron multiplier detector for monitoring the composition of the exit stream from the furnace.

Argon or nitrogen (purity $\geq 99.99\%$) is used as the primary gas in each experiment. Prior to each experiment, the furnace is evacuated at room temperature to 50 millitorr and then backfilled with $N_2$ or Ar at room temperature. Next, the furnace is evacuated and heated to 200°C for 20 min to remove gases weakly adsorbed by the graphite elements and insulation. The furnace is then filled with the desired gas or gas mixture at a constant flow rate of 6 liter/h and 1 atm total pressure. The mass spectra were monitored as a function of temperature for a constant heating rate of 25°C/min and for hold periods at different temperatures.

## 3. Reaction chemistry and analysis of gas-phase concentration by mass spectrometry

Preliminary experiments with inert carrier gases in the graphite furnace indicated that reactions involving carbon and oxygen were occuring as a function of temperature. For the species CO, $CO_2$, $O_2$, and C, two reactions can be written:

$$C + O_2 = CO_2 \quad (1)$$

$$CO_2 + C = 2CO \quad (2)$$

Two other reactions, $2CO + O_2 = 2CO_2$, and $2C + O_2 = 2CO$, can be obtained by linear combination of reactions 1 and 2 and are thus not independent. In order to convert between absolute concentrations, number of moles, and partial pressures, it is convenient to work in terms of the reaction coordinates, $\varepsilon_1$ and $\varepsilon_2$, for the two reactions. For a differential change in the number of moles of species $i$, $dn_i$, appearing in reactions 1 and 2, the following relationships hold from stoichiometry:

$$dn_{CO_2} = d\varepsilon_1 - d\varepsilon_2 \quad (3)$$

$$dn_{CO} = 2d\varepsilon_2 \quad (4)$$

$$dn_{O_2} = -d\varepsilon_1 \quad (5)$$

Integration of Equations 3–5 from an initial state to a final equilibrium state leads to

$$n_{CO_2} = \varepsilon_1 - \varepsilon_2 + n^0_{CO_2} \quad (6)$$

$$n_{CO} = 2\varepsilon_2 + n^0_{CO} \quad (7)$$

$$n_{O_2} = -\varepsilon_1 + n^0_{O_2} \quad (8)$$

where $n^0_i$ indicates the initial number of moles of species $i$. The total number of moles in the gas phase is then

$$n_{Total} = \varepsilon_2 + n^0 \quad (9)$$

where

$$n^0 = n^0_{CO_2} + n^0_{CO} + n^0_{O_2} + n_{inert} \quad (10)$$

Equations 6–10 thus account for the total number of moles present and the extent to which the coupled reactions have proceeded. The term $n_{inert}$ in Equation 10 takes into account the use of a carrier gas such as argon that does not participate in the reaction network.

The equilibrium constants for reactions 1 and 2, $K_1$ and $K_2$, can be written as

$$K_1 = \frac{P_{CO_2}}{a_C P_{O_2}} \quad (11)$$

$$K_2 = \frac{P^2_{CO}}{a_C P_{CO_2}} \quad (12)$$

where $P_i = (n_i / n_{Total}) \times P_{Total}$ is the partial pressure of species $i$, $P_{Total}$ is the total pressure, and $a_i$ is the activity of species $i$. The use of partial pressures in Equations 11 and 12 instead of concentrations results from assuming ideal gas behavior. The validity of ideal behavior for gases at pressures of one atmosphere and temperatures from 300–2000 K can be assessed by computation of the compressibility factor, $Z$, for each gas species. For the experimental conditions examined here, $Z$ is very near unity, principally because of the low reduced pressure, and thus the assumption of ideal gas behavior is warranted. The activity of carbon, which is present in excess, is taken as unity.

The equilibrium constants in Equations 11 and 12 can be rewritten in terms of the reaction coordinates and initial number of moles present to eliminate the partial pressures. This leads to the following set of coupled, non-linear equations for the equilibrium constants:

$$K_1 = \frac{\varepsilon_1 - \varepsilon_2 + n^0_{CO_2}}{-\varepsilon_1 + n^0_{O_2}} \tag{13}$$

$$K_2 = \frac{\left(2\varepsilon_2 + n^0_{CO}\right)^2}{\left(\varepsilon_2 + n^0\right)\left(\varepsilon_1 - \varepsilon_2 + n^0_{CO_2}\right)} \tag{14}$$

The equilibrium constants for these reactions as a function of temperature can be obtained from standard references [22], and then the extents of reaction can be obtained from the solution of Equations 13 and 14. The values of $\varepsilon_1$ and $\varepsilon_2$ thus obtained can be used with Equations 6–10 to determine the equilibrium number of moles, and thus partial pressures, of the individual species.

To obtain the concentration of the gas-phase species from the mass spectrometer data, the following approach was used. Because of gas ionization within the mass spectrometer, multiple peaks, which correspond to fragments of a given parent compound, occur at specific values of the mass/charge ratio, $m/z$. The values of $m/z$ for some parent compounds are listed in Table I, where it can be seen that for some values of $m/z$, more than one compound may be the origin of the signal, e.g., both CO and $N_2$ appear at $m/z = 28$. The fragmentation factors, $\alpha_{Ai}$, (fraction of total ions of species A that occur at mass/charge ratio $i$) of some selected species such as CO, $N_2$, Ar, $CO_2$ and $O_2$ are reported in Table II as measured by the mass spectrometer. The total intensity of the parent peak of a given species $A$, $I_{A,T}$, relative to the intensity of the cracked products at $m/z = i$, $I_{Ai}$, is then given by:

$$I_{A,T} = \frac{I_{Ai}}{\alpha_{Ai}} \tag{15}$$

In instances where two or more compounds may appear at the same value of $m/z$, e.g., CO and $N_2$ at $m/z = 28$, the intensities and ratios of the fragments at $m/z = 12$ (C), 14 (N), and 16 (O) may be used to identify the compounds.

TABLE I Mass-to charge ratio ($m/z$) of selected species

| $m/z$ | Species |
|---|---|
| 46 | $NO_2$ |
| 44 | $CO_2$, $N_2O$, SiO |
| 40 | Ar |
| 32 | $O_2$ |
| 30 | NO |
| 28 | CO, $N_2$, Si |
| 26 | CN |
| 20 | Ar |
| 18 | $H_2O$ |
| 17 | $NH_3$, OH |
| 16 | O, $NH_2$ |
| 14 | N |
| 12 | C |

TABLE II Ionization probability and fragmentation factors for selected species

| Species | $m/z$ | Relative ionization sensitivity ($\beta$) | Fragmentation factor ($\alpha$) |
|---|---|---|---|
| CO | 28 | 1.05 | 0.930 |
| | 16 | – | 0.029 |
| | 12 | – | 0.036 |
| $CO_2$ | 44 | 1.4 | 0.853 |
| | 28 | – | 0.069 |
| | 16 | – | 0.057 |
| | 12 | – | 0.021 |
| Ar | 40 | 1.2 | 0.945 |
| | 20 | – | 0.055 |
| $O_2$ | 32 | 1.0 | 0.731 |
| | 16 | – | 0.269 |
| $N_2$ | 28 | 1.0 | 0.855 |
| | 14 | – | 0.145 |

The sensitivity of the mass spectrometer to nitrogen is $S = 2800$/mtorr.

To convert from intensity data to partial pressures, we express the partial pressure, $P_A$, of parent compound $A$ in terms of the intensity, $I_{Ai}$, as:

$$P_A = \frac{I_{Ai}}{\alpha_{Ai}} \frac{\alpha_{N_2}}{\beta_A TF_i DF_i S} \tag{16}$$

where $\alpha_{N_2}$ is the fragmentation factor for $N_2^+$ ions, $\beta_A$ is the ionization probability of species $A$, $TF_i$ is the transmission factor of species $i$ (equal to $28/M$, where $M$ is the molecular weight), $DF_i$ is the detection factor of species $i$, taken as unity, and $S$ is the sensitivity for nitrogen. Values for $\alpha$ and $\beta$ for the major species under investigation here are listed in Table II. Equation 16 can thus be used with intensity data recorded for cracked species to deconvolute the contributions of multiple species which appear at a single value of $m/z$.

## 4. Results and discussion

### 4.1. Background reactions in argon

The first results pertain to an experiment in which argon was the gas flowing in the furnace, and the temperature was ramped at 25°C/min to 1400°C, held at 1400°C for 10 minutes, cooled at 50°C/min to 1000°C, followed by free cooling to room temperature. Fig. 2 illustrates the time dependence of the temperature and the intensity of different $m/z$ signals recorded by the mass spectrometer. At low temperature near $t = 0$, the baseline intensities of all the species are flat and correspond to the background values of these species in the carrier gas. The ratio of $m/z = 28$ ($N_2$) to $m/z = 32$ ($O_2$) is very different from the 4 : 1 ratio expected for air, and thus a leak of air into the furnace is not occurring.

As the temperature is raised, $m/z = 44$ ($CO_2$) and $m/z = 18$ ($H_2O$) are evolved between $T = 30$–800°C, and at the same time, $m/z = 32$ ($O_2$) is being consumed. The integrated amount of carbon dioxide is approximately three times that of water over this temperature range. The mass-to-charge ratios of species corresponding to fragments exhibit the same general trends as the parent compounds. Thus, we see that the profile of $m/z = 17$ (OH) is very similar to that of the

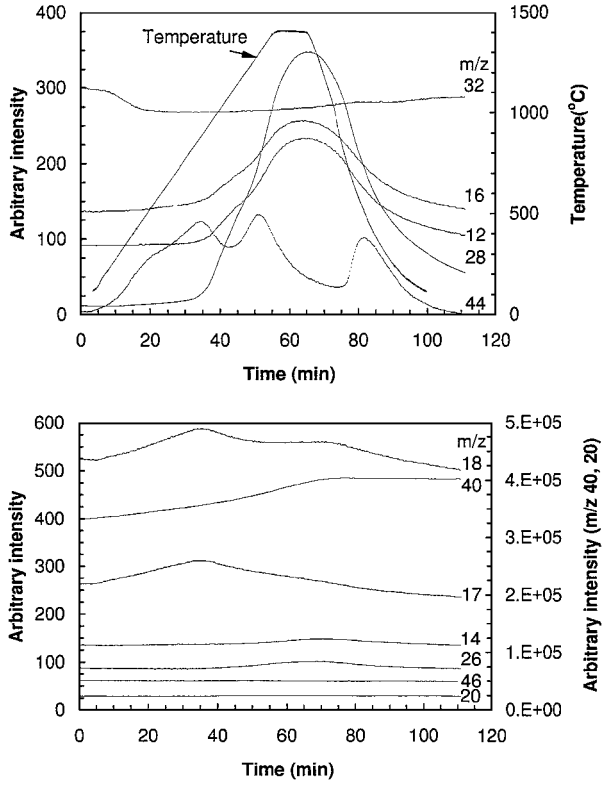


*Figure 2* Temperature and intensity versus time for a heating cycle conducted in a graphite furnace with argon as the carrier gas. To separate the signals for clarity in viewing, the following operations were performed to the recorded intensities: $m/z = 44$ (subtracted 90), $m/z = 32$ (added 120), $m/z = 14$ (added 20), $m/z = 28$ (multiplied by 0.1, then subtracted 20).

parent compound water at $m/z = 18$. The appearance of water is attributed to the desorption of this species from the graphite insulation. The appearance of carbon dioxide with the consumption of oxygen is taken as evidence that the oxidation of carbon (reaction 1) is operative. The appearance of multiple peaks in the $m/z = 44$ profile over this temperature range suggests that carbon dioxide is formed from carbon sources of different reactivity.

During the temperature ramp above 800°C and into the hold period at 1400°C, the intensity of $m/z = 44$ first decreases slightly, and then increases before finally decreasing to near its baseline value. At temperatures greater than 800°C, increases in the signals corresponding to $m/z = 12$, 16, and 28 appear. Because $m/z = 28$ could originate from either $N_2$ or CO, the cracking patterns must be used to identify the compound. Because very little $m/z = 14$ (N) is observed and because $m/z = 12$ (C) and $m/z = 16$ (O) are observed in amounts corresponding to the fragmentation factors in Table II, the $m/z = 28$ species is assigned to CO. This assignment was verified by simulating the production of $m/z = 28$ from each of the cracked intensities at $m/z = 12$ and 16. Fig. 3 shows that the simulated intensities agree well with the observed evolution of $m/z = 28$. The large intensity of carbon monoxide suggests that oxygen is present in the furnace and that this oxygen reacts with the graphite to ultimately form CO at high temperature.

During the hold period, a small amount of $m/z = 26$ is evolved at low concentration. This may assigned to either cracked or doubly ionized cyanogen, $(CN)_2$, which is known to be involved in reaction networks involving carbon and nitrogen at elevated temperatures. As the furnace is cooled, the amount of carbon monoxide decreases and a peak corresponding to carbon dioxide appears. As room temperature is approached, the intensities of the species approach the baseline values observed at the start of the experiment.

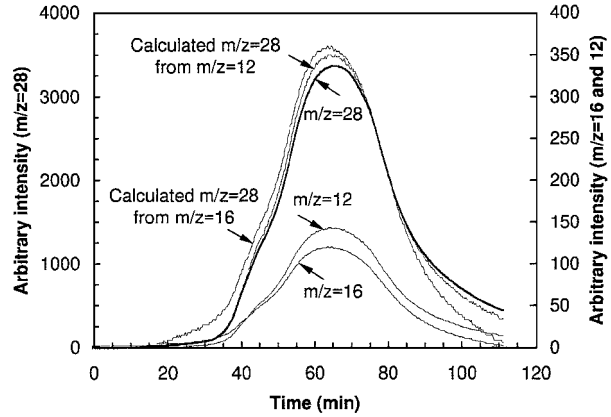


*Figure 3* Comparison of the experimental and simulated intensities for $m/z = 28$. The spectra for $m/z = 28$ were separately calculated from $m/z = 12$ and 16 by using the fragmentation factors listed in Table II.

The occurrence of $CO_2$ and CO over a range of temperatures along with changes in the oxygen signal indicate that reactions 1 and 2 are occurring in the furnace. These reactions are driven in part by the presence of trace oxygen in the argon carrier gas, and reaction of this oxygen with carbon leads to $CO_2$ at low temperature. The amount of oxygen consumption, however, is a factor of 2–3 less than would be predicted by the stoichiometry of reaction 1. This lack of closure of the carbon and oxygen balance is even more pronounced above 800°C, where the amount of CO that is produced is substantially above what would be predicted by the level of oxygen consumption.

To aid in the interpretation of the data in Fig. 2, the equilibrium concentrations for the species appearing in the coupled reactions 1 and 2 were solved by numerical methods. The input into the model was an initial concentration of oxygen $I_{O_2} = 30$ corresponding to the background level of consumption measured by the mass spectrometer. Fig. 4 illustrates the equilibrium concentrations (converted to units of intensity from the mass spectrometer from Equation 16) of $CO_2$, CO and $O_2$ over a range of temperature. At temperatures below 300°C, $CO_2$ is the dominant equilibrium product whereas at much higher temperature, CO is the dominant species. The oxygen, which is never present in large amounts because of the excess of carbon, is present either as CO or $CO_2$. The simulations in Fig. 4 have a number of similarities with the data obtained in the experiments in Fig. 2 and capture the main features in that $CO_2$ is the primary product at low temperature whereas CO is the main high-temperature product.

The major differences between the data in Fig. 2 and the equilibrium simulations in Fig. 4 can be explained, in part, by the effects of reaction kinetics. At low temperature in the experiments, no $CO_2$ is produced until above 100°C, presumably because the reaction

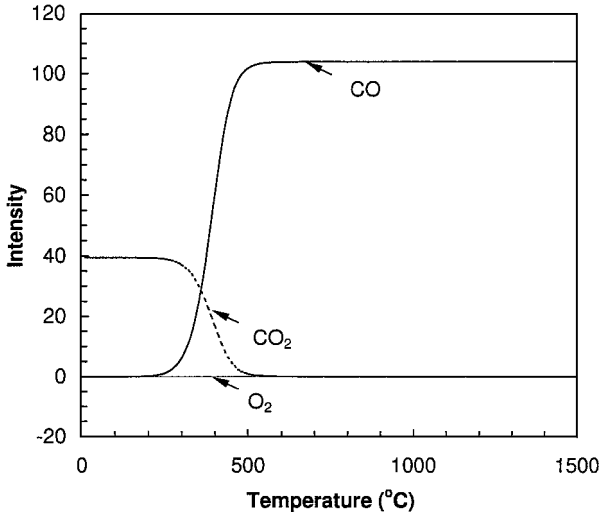


*Figure 4* Simulated equilibrium concentrations of the gas-phase species for the coupled reactions $C + O_2 = CO_2$ and $CO_2 + C = 2CO$ using an initial concentration of $I_{O_2} = 30$ corresponding to the consumption of $O_2$ observed in the experiment. The partial pressures were converted into units of intensity for direct comparison with the data obtained in the experiments.

proceeds according to an activated rate law. The temperature at which the crossover in relative amounts of $CO_2$ and CO occurs is also not well described by the equilibrium model. This, too, can be rationalized in terms of kinetics; further support for not always being at equilibrium is evidenced by the features in the $CO_2$ profile in Fig. 2 which suggest different carbon species with different reactivity, i.e., a kinetic limitation. Thus, we see that the equilibrium model can be used to help identify which species are thermodynamically favored at low and high temperature but cannot be used to describe all of the features of the reaction kinetics observed in the experiment.

Although the dominant species at high and low temperature are correctly predicted by the equilibrium model, more $CO_2$ at low temperature and much more CO at high temperature is seen in the experiments than can be rationalized by oxygen consumption and the reaction stoichiometry. We attribute the source of the extra carbon-containing compounds to the presence of oxygen adsorbed by the high-surface area graphite insulation in the colder parts of the furnace which is desorbed as the temperature is raised. If this interpretation is correct, then the production of these species should have a transient component, and the intensity of $CO_2$ and CO should diminish with time as the adosorbed oxygen is consumed from the system.

To test this hypothesis, the furnace was cycled from 50°C to 1400°C in the saw tooth pattern indicated in Fig. 5. The intensities corresponding to $m/z = 44$, 32, 28, 16 and 12 are shown as well and they vary in a similar fashion as to what was observed in Fig. 2. The main difference, however, is that with time, the intensities of $m/z = 44$ and 28 decrease by a factor of six whereas the $m/z = 32$ intensity decreases by less than a factor of two. The behavior of these three masses suggests that oxygen is present in the furnace in large amount and is consumed during the cyclic heating pattern. The oxygen leading to $CO_2$ and CO above room temperature does not appear in the $m/z = 32$ signal because

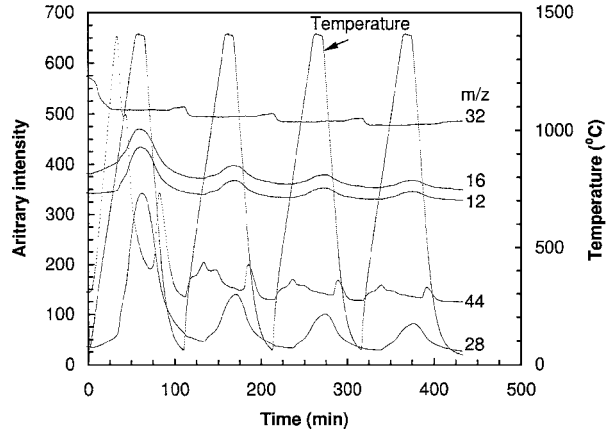


*Figure 5* Temperature and intensity versus time for a saw-toothed heating cycle conducted in a graphite furnace with argon as the carrier gas. To separate the signals for clarity in viewing, the following operations were performed to the recorded intensities: $m/z = 44$ (added 50), $m/z = 32$ (added 350), $m/z = 16$ (added 250), $m/z = 12$ (added 250), $m/z = 28$ (multiplied by 0.1).

it is only evolved from the colder parts of the furnace at elevated temperature, where it reacts to form either $CO_2$ or CO. Further support for this interpretation is that more CO is produced than $CO_2$ as a consequence of more oxygen being desorbed from the graphite at high temperature.

## 4.2. Background reactions in nitrogen

The data in Figs 2–5 are for the reactions observed in experiments that were conducted with argon as the carrier gas. A second type of experiment was conducted with nitrogen as the carrier gas. Fig. 6 shows that the

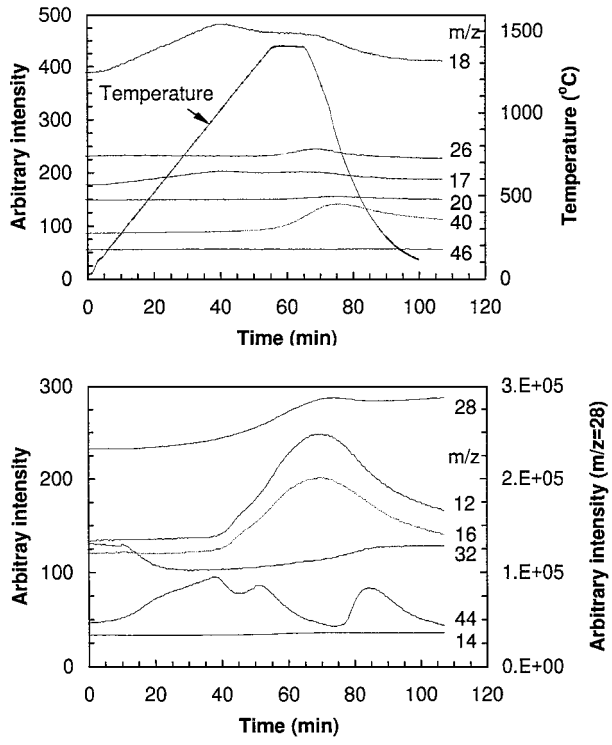


*Figure 6* Temperature and intensity versus time for a heating cycle conducted in a graphite furnace with nitrogen as the carrier gas. To separate the signals for clarity in viewing, the following operations were performed to the recorded intensities: $m/z = 20$ (added 30), $m/z = 28$ (added 40,000), and $m/z = 44$ (subtracted 30).

intensities of $m/z = 44$, 18 and associated fragmentation species are very similar as to what was observed in Fig. 2. The major difference, however, is that the $m/z = 28$ peak now appears as a smaller signal above the large signal corresponding to the nitrogen carrier gas used in the experiment. The assignment of the $m/z = 28$ peak to CO is still valid, however, as a consequence of the $m/z = 12$ and 16 signals accompanying it, and this was again verified by simulation. Thus, the evolution of small amounts of CO above a large $m/z = 28$ background arising from $N_2$ can be observed by monitoring the intensities of the C and O fragments of the parent CO compound.

Taken together, the results in Figs 2 and 6 indicate that the background chemistry occuring in the furnace is fairly complex, even when no sample is present. The underlying mechanism suggested by these data is the following. At low temperature, oxygen present in the carrier gas and in the furnace reacts with the graphite to form $CO_2$, which is the dominant species predicted by equilibrium. At still higher temperatures, the residual oxygen reacts with the graphite to form relatively large amounts of CO. The amount of $CO_2$ and CO produced, however, is much more than would be predicted by the reaction stoichiometry from the consumption of oxygen. Thus, we conclude that the furnace has some adsorptive capacity for oxygen which is not released until higher temperature and appears as $CO_2$ and CO; the intensity of these signals decreases with time as the source oxygen is consumed from the furnace. This high temperature desorption is also evident in the $m/z = 40$ (argon) signal in Fig. 6. The appearance of argon at high temperature, which was not used in the experiment, further attests to the difficulty in removing these adsorbed species. A variety of other purge and evacuation cycles were examined, but these were unsuccessful in removing the majority of the adsorbed gases. Although heating to 1400°C is successful in significantly reacting away the oxygen (see Fig. 4), the necessity of doing this at such high temperature precludes its use as a pretreatment purge strategy.

### 4.3. Decomposition reactions at high temperature

To assess the capability to observe high-temperature gas-phase reaction products above the baseline of background intensities, a sample of $CaCO_3$ was heated to 1200°C in argon and held for 1 hour. Fig. 7 displays the intensity of signals evolved for the gas-phase species as well as the degree of shrinkage versus temperature, as recorded by the dilatometer. At 650°C, substantial shrinkage of the sample begins which coincides with the evolution of a signal at $m/z = 44$; this can be assigned to $CO_2$ based on the cracking patterns. The sintering of the sample is thus seen to be strongly correlated with the decomposition reaction $CaCO_3 = CaO + CO_2$. Sintering of the sample continues throughout the hold at 850°C but then slows appreciably until the temperature is raised to 1200°C. During the latter stage of shrinkage, the decomposition product observed in the gas-phase is at $m/z = 28$, which can be assigned to CO based on the fragment patterns at $m/z = 12$ and 16. The appearance

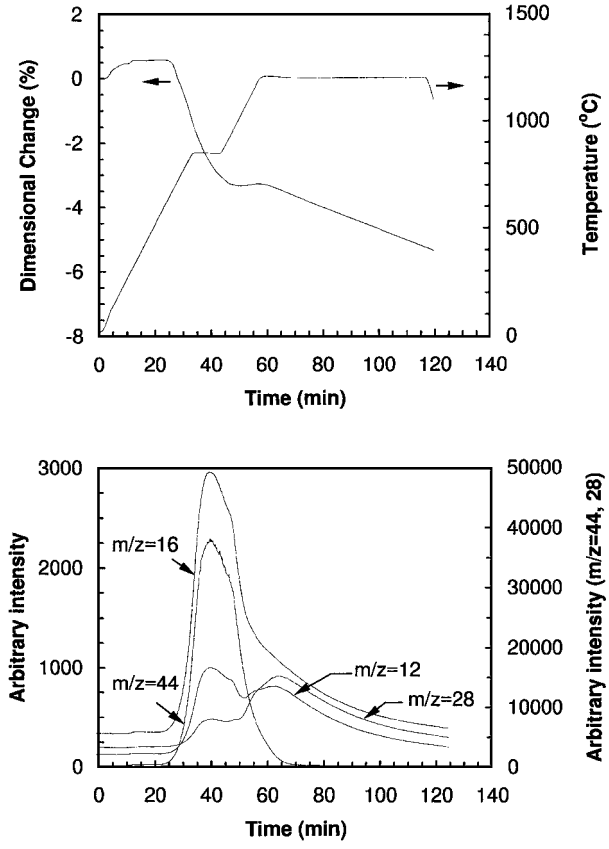


*Figure 7* Temperature, shrinkage, and intensity versus time for a heating cycle conducted in a graphite furnace with argon as the carrier gas for a sample of $CaCO_3$.

of CO at elevated temperature arises from the conversion of the $CO_2$ from decomposition into CO, according to the equilibrium reactions 1 and 2.

The intensity of the $m/z = 44$ and 28 signals can be integrated quantitatively using Equation 16 to determine the number of moles of $CO_2$ produced by the decomposition of $CaCO_3$. This amounts to 6.31 millimoles of $CO_2$ and is within 5% of the number of moles determined from the measured weight loss of the sample and from the stoichiometry of the decomposition reaction. Based on the sensitivity of the mass spectrometer, a signal of approximately 100 ppm in the furnace effluent stream can be detected above the background reactions.

The next phase of this work will be to combine the analysis of gas-phase chemistry with the sintering of samples and microstructural development. Such studies will be conducted in inert gases as well as in gases such as CO and $CO_2$ which may participate in the high-temperature reaction network. The presence of the CO and $CO_2$ is expected to change the gas-phase chemistry prevailing in the furnace and may influence the sintering kinetics or microstructural development of the ceramic or both.

## 5. Conclusions

The gas-phase chemistry occurring at high temperature in a graphite furnace/dilatometer was examined by mass spectrometry. The reactions taking place were seen to involve oxygen, carbon, carbon dioxide, and carbon monoxide. The presence of the oxygen was attributed to trace impurities in the carrier gases and to

adsorption of oxygen on the graphite insulation. At low temperature, carbon dioxide was the favored reaction product, and at high temperature, carbon monoxide was the main compound observed. Additional species observed were water and cyanogen. The appearance of carbon dioxide at low temperature and carbon monoxide at high temperature is qualitatively consistent with the simulated results obtained from the solution of the coupled equilibrium relations.

## Acknowledgment

Partial support for this work was obtained from the University of Missouri Research Board.

## References

1. J. L. MARGRAVE, "The Characterization of High-Temperature Vapors" (John Wiley & Sons, New York, 1967).
2. J. H. HASTIE, "High Temperature Vapors: Science and Technology" (Academic Press, New York, 1975).
3. *Idem*., "Characterization of High Temperature Vapors and Gases," Vol. 1 (NBS Special Publication 561, US Department of Commerce, 1979).
4. G. A. SOMORJAI, in "Advances in High Temperature Chemistry," Vol. 2, edited by L. Eyring (Academic Press, New York, 1969) p. 203.
5. P. ROCABOIS, C. CHATILLON and C. BERNARD, *J. Amer. Ceram. Soc*. **79** (1996) 1351.
6. S.-S. LIN, *ibid*. **58** (1975) 160.
7. M. A. MULLA and V. D. KRSTIC, *J. Mater. Sci*. **29** (1994) 934.
8. T. GRANDE, H. SOMMERSET, E. HAGEN, K. WIIK and M. EINARSRUD, *J. Amer. Ceram. Soc*. **80** (1997) 1047.
9. W. VAN RIJSWIJK, *ibid*. **73** (1990) 148.
10. W. J. CLEGG, *ibid*. **83** (2000) 1039.
11. E. A. NESS and W. RAFANIELLO, *ibid*. **77** (1994) 2879.
12. H. WADA, M.-J. WANG and T.-Y. TIEN, *ibid*. **71** (1988) 837.
13. F. L. RILEY, *ibid*. **83** (2000) 245.
14. U. NEIDHARDT, H. SCHUBERT, E. BISCHOFF and G. PETZOW, *Key Engineering Materials* **89–91** (1994) 187.
15. C. BOBERSKI, H. BESTGEN and R. HAMMINGER, *J. Eur. Ceram. Soc*. **9** (1992) 95.
16. J. JUNG, *Keramische Zeitschrift* **42** (1990) 830.
17. O. ABE and S. KANZAKI, *J. Ceram. Soc. Japan* **97** (1989) 187.
18. M. L. MECARTNEY, *J. Mater. Sci. Lett*. **6** (1987) 370.
19. H.-J. KLEEBE, W. BRAUE and W. LUXEM, *J. Mater Sci*. **29** (1994) 1265.
20. S. SIEGEL, M. HERMANN and G. PUTZKY, *Key Engineering Materials* **89–91** (1994) 237.
21. H. NANRI, SH. ISHIDA, N. TAKEUCHI, K. WATANABE and M. WAKAMATSU, *J. Soc. Mat. Sci. Japan* **45** (1996) 694.
22. Journal of Physical and Chemical Reference Data. Monograph; No. 9. NIST-JANAF Thermochemical Tables/Malcolm W. Chase, Jr. (American Chemical Society, Washington, D.C.; American Institute of Physics for the National Institute of Standards and Technology, Woodbury, N.Y. 1998).

*Received 24 May 2001*
*and accepted 25 February 2002*